HANSER

Sample Pages

Goerg H. Michler, Francisco J. Baltá-Calleja

Nano- and Micromechanics of Polymers

Structure Modification and Improvement of Properties

ISBN: 978-3-446-42767-9

For further information and order see

http://www.hanser.de/978-3-446-42767-9

or contact your bookseller.

4 Crazing

4.1 The Phenomenon of „Craze“

As mentioned in the previous chapter, plastic deformation of polymers is a heterogeneous process, concentrated in local zones. Local plastic processes appear in form of shear bands, void formation with fibrillation, inter- and intraspherulitic deformation, and formation of crazes. Crazing has been intensively investigated over the last 60 years, with major reviews appearing regularly [1–8]. It is usually assumed that crazes are typical of amorphous, glassy polymers, such as PS, SAN, and PMMA, which are brittle at room temperature with elongation at break of a few percent. The reason is that crazes are visible in the amorphous, glassy polymers during mechanical loading with the eye in reflected light (see Fig. 4.1). Their macroscopic appearance of cracks left these zones with the name of craze. “Craze” is an old English word for hairline crack. Synonyms include “craquele” (from the pattern of cracks in the glaze of porcelain (china) or pottery, microcracks and “silver cracks” (from the Russian name).

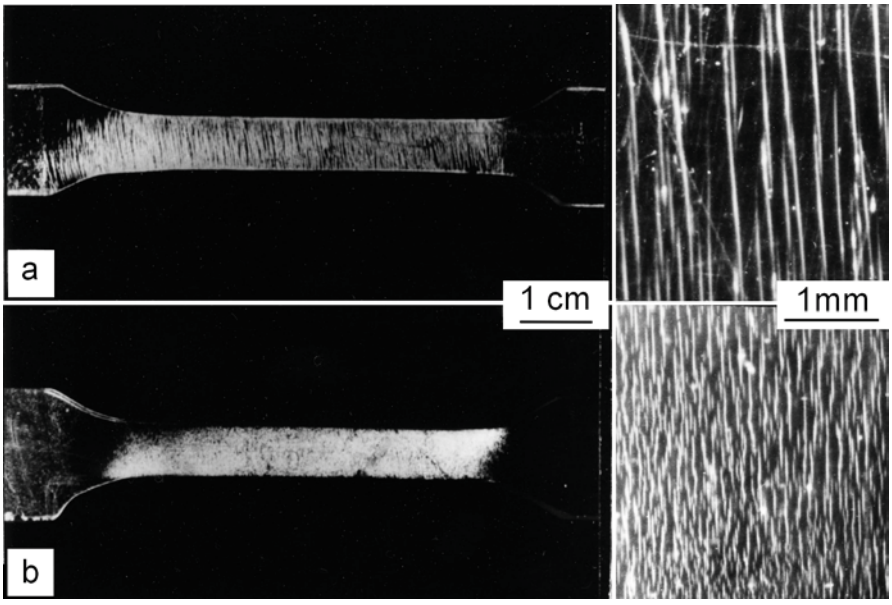

FIGURE 4.1 Tensile bars after loading in overview (left) and low optical magnifications of the bars (right); a) polystyrene; b) poly(methylmethacrylate)

Several crack-like zones

The formation of crack-like zones in brittle materials under stress is a very general phenomenon, which is observed in very different materials:

- *Inorganic glasses* are typical examples of amorphous brittle materials with very fast crack propagation. However, electron microscopic investigations of pre-crack areas revealed small plastically deformed zones up to a few micrometers long. These zones contain small voids and plastically deformed fibrils, which consist of stretched interconnected SiO_4 tetraeders [9].
- *Amorphous metals* (or metallic glasses) are formed following extreme cooling from the melt of some metal alloys. They show local plastic zones during loading in tension of some 10 μm length and up to 1 μm thickness [10].
- Crack formation and propagation in *metals* is often connected with the formation of microvoids and plastically stretched material between the voids. Such zones resemble coarse crazes.
- In *drying mud, starch mash,* or cooling down lava shrink stresses are built up, yielding a macroscopic crack pattern [11]. Figure 4.2 shows a typical crack pattern in dried mud. With continuous drying, shrinkage stresses increase, creating thick cracks with larger distances first and then step by step thinner and smaller cracks.

FIGURE 4.2 Pattern of thicker and smaller cracks in a dried mud (in the Negev desert in Israel after heavy rain fall)

The craquele pattern in the glaze of china or pottery arises from a similar, but much slower process. The cracks in lava forming during solidification are often organized in a very regular hexagonal pattern. A fracture mechanical analysis provides an explanation of such regular geophysical crack and fracture arrangements [12] and shows an interesting similarity to craze pattern in amorphous polymers. The distance a between the cracks in an elastic body with a Young's modulus E loaded homogeneously with a stress P is given by

$$a = \frac{E \cdot W}{p^2(1 + \nu^2)} \tag{4.1}$$

where W_c = critical energy density and ν = Poisson constant.

Crazes and craze-like zones

With increasing intrinsic stress P, the distance a between cracks decreases. Examples of formation of crack patterns due to shrinkage stresses show only a formal similarity to crazes. Very generally, a craze can be described as a well defined, flat deformation zone filled with highly extended, mostly fibrillar matter and interspersed voids, which appears in amorphous and semicrystalline thermoplastics perpendicular to the main stress axis (see Fig. 4.3, Table 3.1). The first hints concerning the true nature of crazes date from 1949/1950 based on X-ray scattering measurements [13, 14]. With light optical methods it was found that crazes contain deformed, oriented polymer material [15–17]. Notable progress in the discovery of craze microstructures was made through *Kambour* in the 1960s [1, 3, 18] and *Beahan, Bevis* and *Hull* in the beginning 1970s [19–21]. As mentioned earlier, crazes are typical of amorphous, glassy polymers; however, they also appear in more ductile amorphous polymers, in semicrystalline polymers, and in many polymer blends. In addition, many polymers show structured deformation zones, which can be described as craze-like zones [7]. Since many features and initiation steps are similar in different polymers, the main characteristics of crazes are summarized in the following.

4.2 Characteristics of Crazes

Electron microscopy studies of craze structure

The true microstructure of crazes was revealed mainly by electron microscopy, using several preparation and investigation techniques:

- Staining or filling the microvoids inside crazes with chemical agents in the bulk after or during tensile or bending loading, preparation of ultrathin sections, and inspection by TEM [1, 3]. The craze composition of microvoids and stretched fibrils is made visible by those means – cf. Fig. 2.31.
- Studies of stretched ultrathin sections [19] or solution cast films on supporting Mylar films or copper grids in TEM [20, 22].
- Deformation of semi-thin sections directly (without supporting film) in HVEM [7, 23, 24]. The fibrillar structure inside the crazes then becomes clearly visible. Most of the micrographs in this chapter and in other chapters have been taken using this technique.
- Studies of the surfaces of deformed samples or fracture surfaces of bulk materials in SEM [7, 25–27]. The domain-like structures on fracture surfaces can be identified as broken and relaxed fibrils (see Fig. 4.27 and 4.28).

The fibrillar structure of crazes also has been studied using small angle electron diffraction [28] and X-ray scattering techniques [28, 29].

An overview of craze patterns in tensile bars and in front of a crack tip is shown in Figs. 4.1 and 2.37. The typical fibrillar structure inside the crazes in PS can be seen in Fig. 4.3.

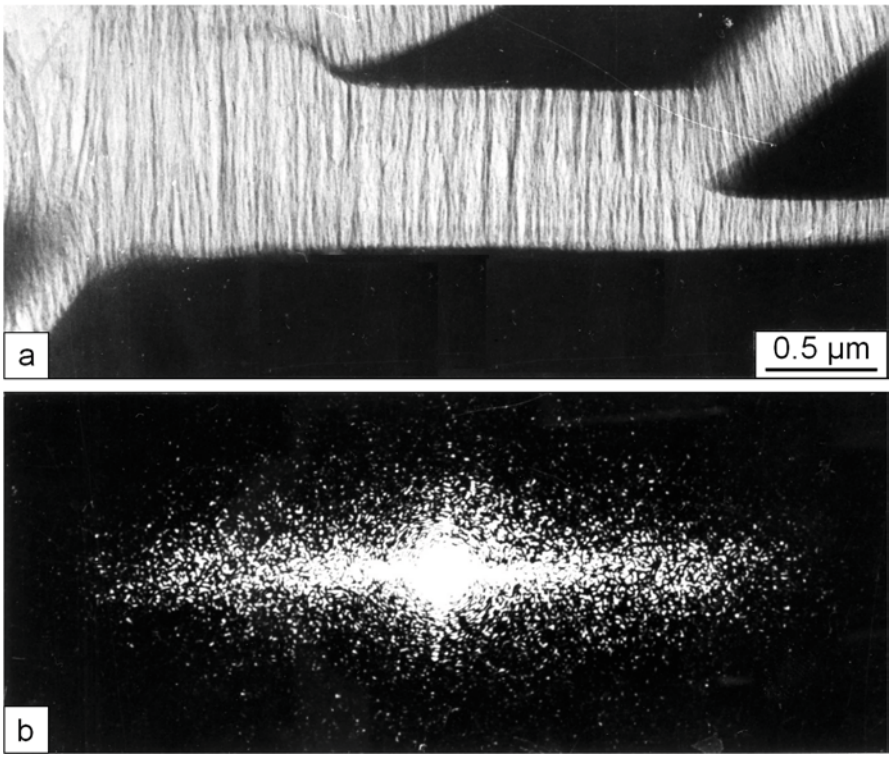

FIGURE 4.3 Interior of a craze in PS with clear fibrillation (stretched 1 µm thick section in HVEM, deformation direction vertical)
a) HVEM micrograph
b) laser diffraction pattern

The laser diffraction pattern in Fig. 4.3b reflects the parallel arrangement of the craze fibrils (the horizontal line of dots perpendicular to the fibrils) and the larger variation of the fibril distances (the scattering of distances of dots from the central spot). The thickness of crazes increases with increasing length of a growing craze and can be illustrated in a "craze thickness profile". Figure 4.4 shows a craze with increasing distance from the craze tip and the corresponding craze thickness profile. The craze thickness D increases up to a few µm with opening angles α (angle between craze boarders) up to about 5°. Usually, the craze thickness is limited due to the presence of other crazes in its vicinity. In front of the regular craze tip (i. e., the beginning fibrillation), a very narrow bright zone about 10 µm long and 25 nm thick, called "pre-craze", is visible [7, 24, 30]. This structure will be discussed in detail together with the processes of craze-initiation in Section 4.4.

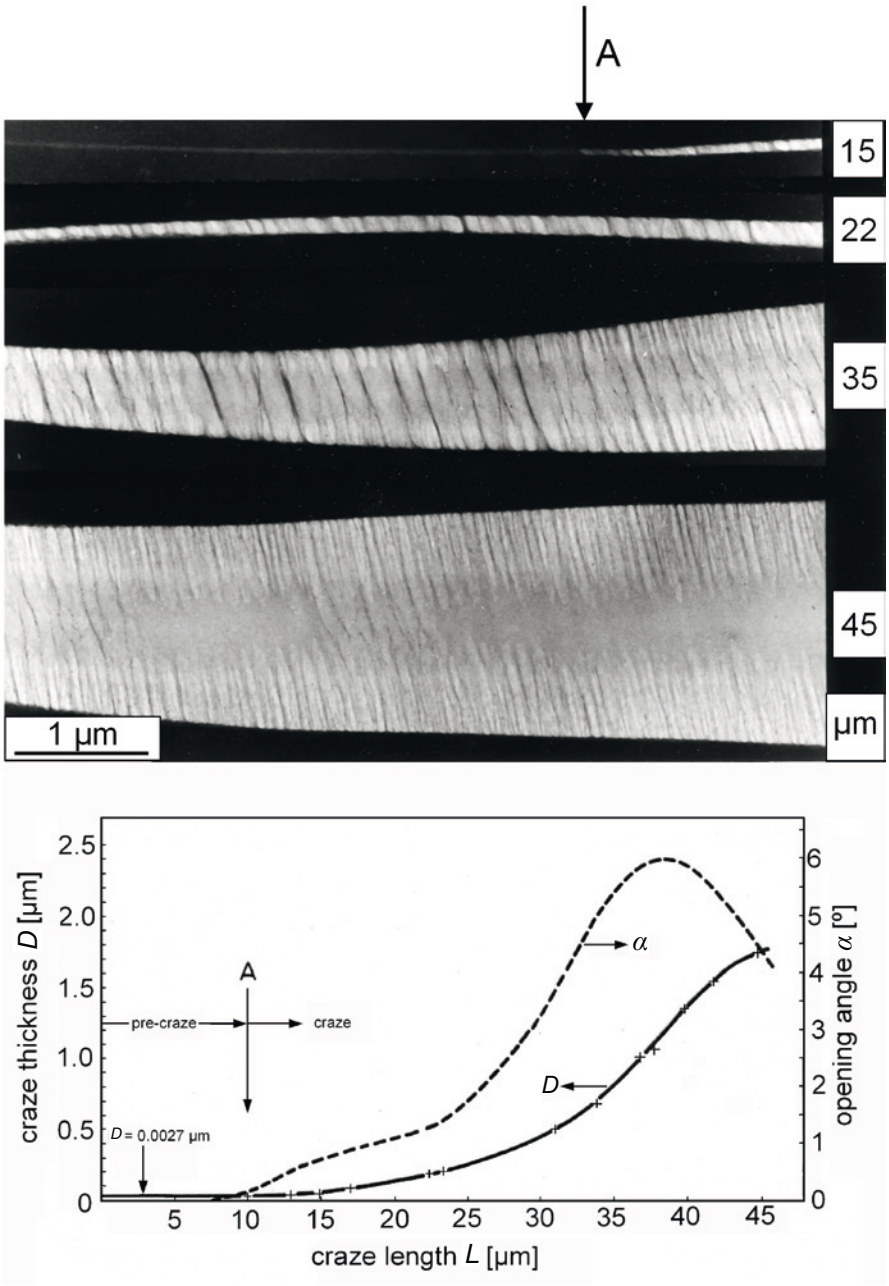

FIGURE 4.4 Structure of a craze in PS in increasing distances from the craze tip; deformation direction vertical, HVEM micrographs; diagram: Craze thickness profile (variation of craze thickness D and opening angle α with increasing craze length L); "A" marks the transition of the pre-craze (about 27 nm thick) to the regular craze

The material inside the craze is strongly plastically deformed up to elongations between 100 and 400%, usually in fibrils [22, 30]. The fibrils are oriented in perpendicular direction to the craze boarders and parallel to the loading direction. Between the fibrils, elongated nanovoids appear with a void content of up to more than 50%. Therefore, crazing is associated with an increase in volume and a decrease in material density. It is remarkable that the transition from the highly deformed craze material to the undeformed (only elastically loaded) polymer material outside the craze is very sharp, often in the range of only 10–20 nm. Craze fibril thicknesses vary from a few nm up to more than 20 nm. However, the dark lines visible in the electron micrographs

(Figs. 4.3 and 4.4) are not identical with the individual single fibrils. In the direction of the electron beam there are many fibrils that cannot be resolved individually. A resulting superposition structure is shown in Fig. 4.5 using a larger magnification with a pattern of shorter dark stripes. A model analysis of contrast development of fibrils, which lie one on top of the other, shows that the smallest visible distances of stripes correlate with the average distances between craze fibrils [30].

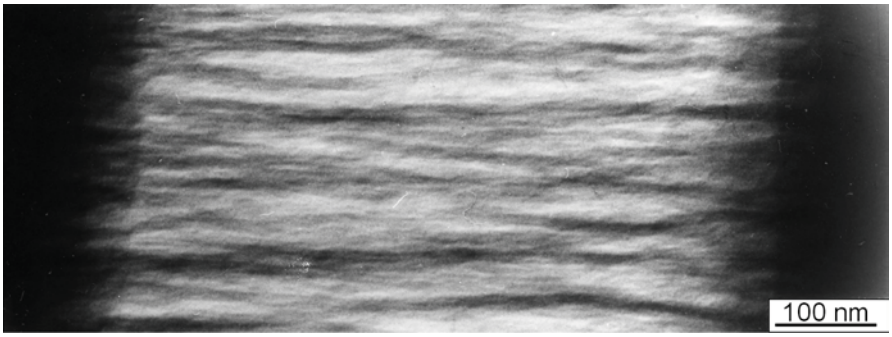

FIGURE 4.5 Larger magnification of the interior of a craze: The apparently visible "fibrils" are superposition structures of many true fibrils (deformation direction horizontal)

In summary, the general structural features of crazes are:

1. Crazes are narrow, long zones of heavily plastically stretched and often fibrillated polymer material.
2. They are oriented with the longitudinal direction (growth direction) perpendicular to the main deformation direction.
3. They show relatively sharp boundaries to the undeformed polymer material.

Some differences between crazes, cracks, and shear bands are mentioned in Section 3.3 in Table 3.1. The most remarkable difference to cracks is the load bearing efficiency of the stretched craze fibrils. This property of the fibrils can be demonstrated using an ultra-microindentation hardness measurement at a crack tip with a craze ahead (see Fig. 4.6). In front of the crack with a lower microhardness (values different from zero arise from the interaction of the indenter with the crack boundary) the microhardness increases rapidly and reaches the bulk microhardness value in front of the craze [32]. The microhardness inside the craze is higher than that of the bulk polymer because of the stretched, load bearing fibrils, which overcompensate the voids in between.

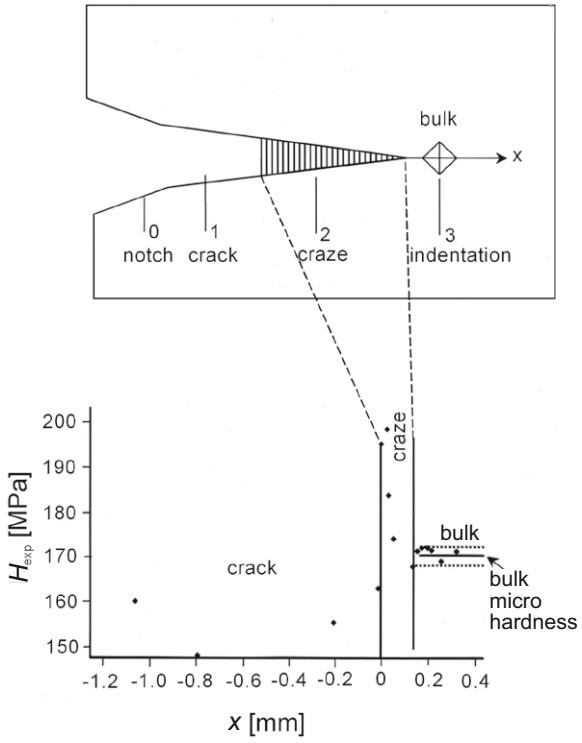

FIGURE 4.6 Microindentation hardness values measured along the crack propagation direction
a) scheme of arrangement of artificial notch (0), crack (1), craze (2) and bulk material (3)
b) corresponding microhardness values

■ 4.3 Variety of Craze Structures

The regular fibrillation inside a craze is often assumed as the characteristic craze structure. However, very different structures in different polymers, even in PS, can appear. Examples of the variety of craze structures in PS from a finely fibrillated network to larger voids are shown in Fig. 4.7. A characteristic feature of many crazes is a brighter zone in the center, the mid-rib (Fig. 4.7 a, b). Different craze structures can appear in the same material, at different stages of growth, or due to different loading conditions (see Section 4.6). Other materials show coarser craze fibrillations, such as PVC (Fig. 4.8) or solvent crazes in PE (stress corrosion crazes, see Chapter 7).

9 Rubber Toughened Polymers

9.1 Overview

A special family of polymer blends, known as *rubber-modified polymers*, exhibit very high toughness. The original approach to producing rubber-modified polymers with enhanced toughness was to combine hard, brittle polymers with soft, rubbery ones, according to the equation "brittle + soft = tough". However, the toughness of optimized rubber-modified polymers does not simply result from combining the properties of their components (as illustrated in the additivity curve (a) in Fig. 8.1). Because of a pronounced morphology and special toughening mechanisms, synergistic effects corresponding to curve (d) in Fig. 8.1 can be realized. Development and production of rubber-modified, high-impact polymers started mainly after the World War II, continuing to be a big field in polymer industry today.

Toughness as a complex property

Toughness is one of the most complex properties and one that is difficult to control, because it is greatly influenced by many morphological and micromechanical parameters. Very simply spoken, the basic aim of any toughening enhancement is to increase the area below the stress-strain curve in tensile or other deformation tests (i. e., the energy absorption during deformation until fracture) (see Fig. 5.15). In general, it is possible to increase the stress σ by suppressing all critical defects and avoiding critical stress concentrations, although this causes a decrease in strain at break (see curve *1* in Fig. 5.15; this is only realized in highly oriented fibers or thin films). The opposite case, a large elongation or strain ε, is usually connected with very low strength values ("softening", curve *2* in Fig. 5.15). Therefore, the optimum case is the combination of relatively high values of stiffness (modulus E), strength σ, and strain ε, as shown in curve *3* in Fig. 5.15. As mentioned before, this situation requires that large, critical defects and stress concentrations are avoided and a particular morphology is realized that permits lots of very small local yielding events (mechanism of true toughening).

Rubber toughening generally refers to the modification of a hard, brittle, glassy polymer (e. g., PS, SAN, PMMA, COC, and PVC) with soft, rubber-like particles. The traditional materials are HIPS (high-impact PS), ABS (acrylonitrile-butadiene-styrene), and ACS (acrylonitrile-chlorinated PE-styrene). A comparable situation occurs when a typically ductile polymer is used at lower temperatures

(below the glass transition temperature, i. e., in the brittle state), resulting in mechanisms of so-called "low-temperature toughness". Both types of toughness can be realized by homogeneous rubber particles, core-shell particles, or heterogeneous modifier particles in so-called *disperse systems*. The rubber content varies usually between 5 and 30 wt.-%. An alternative is a network arrangement of the rubber in *inclusion systems* or *network systems*. Because of the wide application and characteristic micromechanical deformation mechanisms, these polymer blends are discussed separately in Section 9.5. Another group of polymer blends with an enhanced toughness based on the *inclusion yielding mechanism* (*rigid* toughening) is considered in Section 8.4. The large variety of different rubber-modified polymers is discussed in several books and many reviews (e. g., [1–8]).

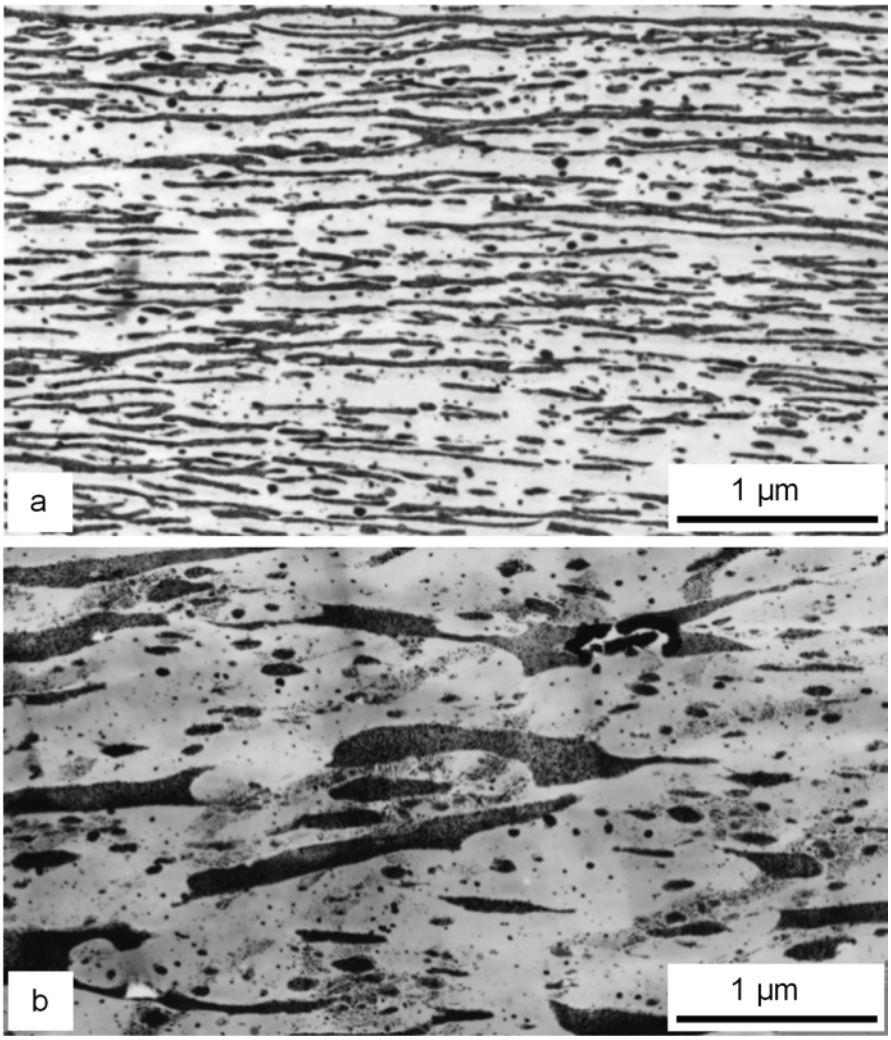

FIGURE 9.1 Injection molded parts of a 80/20 COC/EVA with highly oriented EVA particles at the surface a) and less oriented ones inside the material b) (TEM micrographs, rubber phase stained)

9.2 Morphology

The first rubber-modified polymers were simple mechanical blends of PS and styrene rubber and of SAN with nitrile rubber. Such mechanical (or physical) blends show irregularly shaped rubber particles with a broad particle diameter distribution. Another disadvantage is the low form stability of the rubber particles during processing or manufacturing. An example is shown in Fig. 9.1 with oriented EVA particles inside and particularly in the surface layers of an injection molded part of a COC/EVA (80/20) blend (COC is a norbornene-ethylene copolymer, EVA, ethylene vinylacetate, contains 20 %VAc content). Such oriented rubber particles caused by processing are also visible in HDPE/rubber blends (see Fig. 8.10).

In the case of ABS, the rubber particles are prepared and pre-formed separately, grafted with SAN macromolecules and then mixed with SAN (emulsion polymerization process). Very regularly shaped, spherical particle of a similar size or with a defined bimodality can be prepared (see Fig. 9.2). The effect of grafting is visible on the dotted surface of the particles (surface grafting) and in small white SAN inclusions inside the particles (internal grafting).

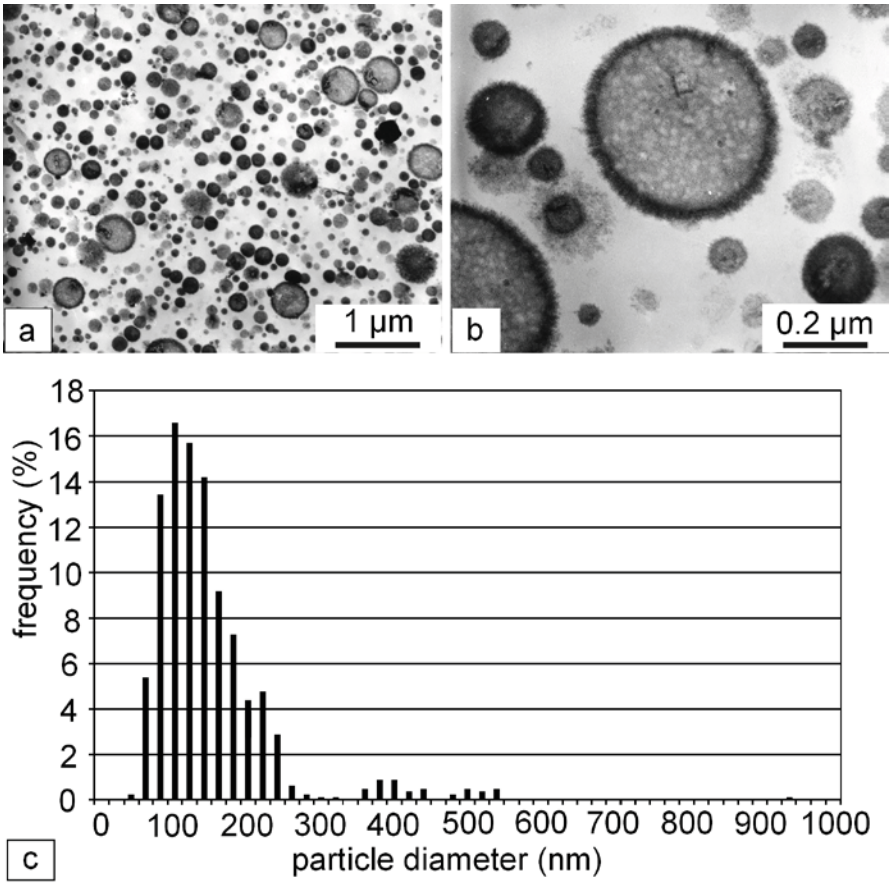

FIGURE 9.2 Size and arrangement of rubber particles in an ABS polymer
a, b) spherical rubber particles, the larger magnification (b) shows the grafted surfaces and small SAN inclusions inside the particles (TEM micrographs);
c) frequency distribution of the rubber particle diameter

Figure 9.3 shows the phase structure of typical high-impact PS (HIPS). During polymerization of PS in the presence of the dissolved rubber, phase inversion takes place, yielding rubber particles with PS inclusions (mass polymerization). Various types of particles can be created, depending on the stirring rate, ranging from the characteristic "salami particles" up to rubber shells (core-shell particles). The grafted surface layer of the rubber particles can also be identified in larger magnifications with a lot of grafted dots – see micrographs a, b. The PS inclusions considerably increase the volume of these particles, enabling a volume content of up to about 30 % with a rubber content of only 7 – 8 wt.-%. It is visible in Fig. 9.3 a, b that a part of the larger salami particle

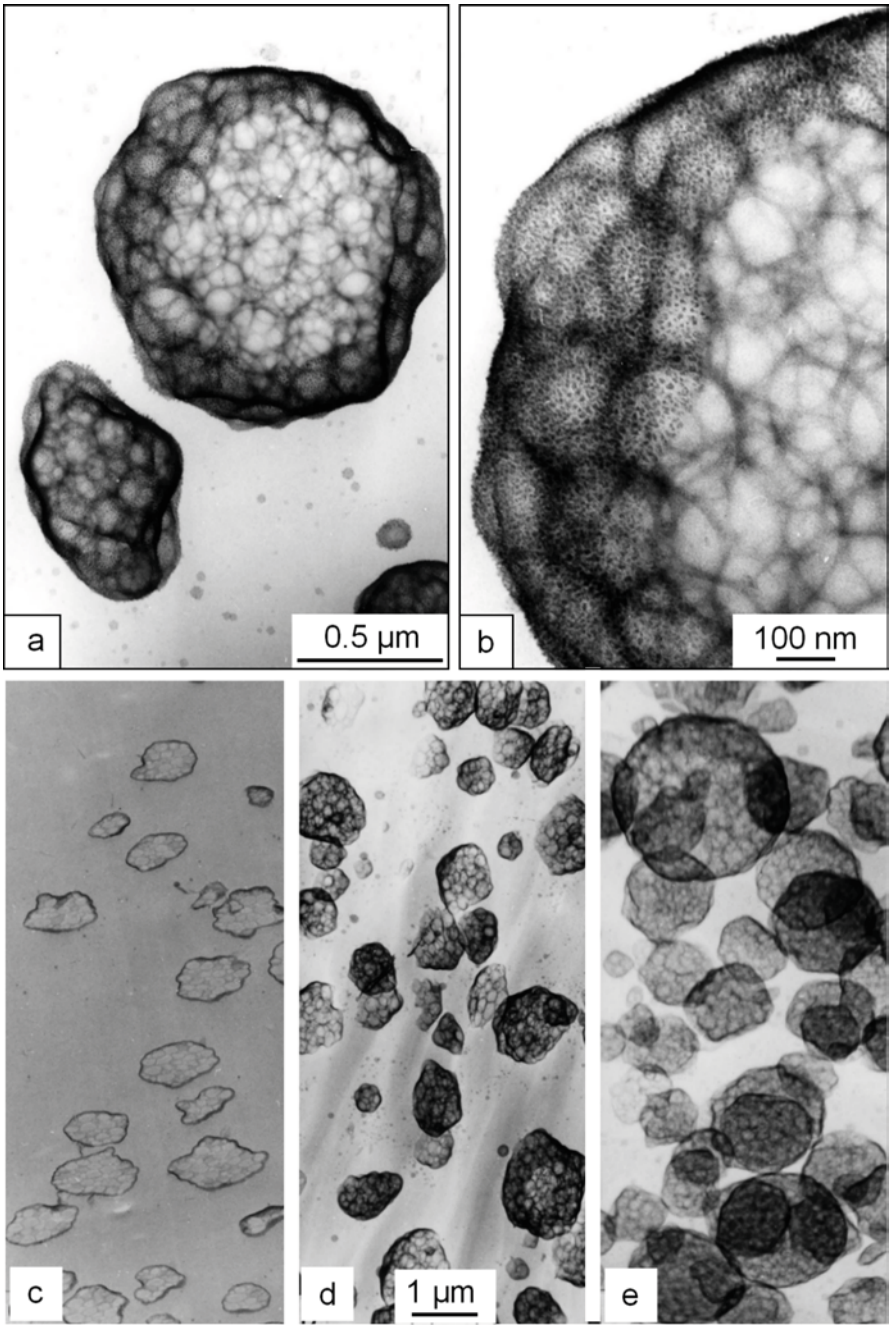

FIGURE 9.3 Salami particles in HIPS; a, b) visible in a 0.5 µm thick section with grafted interface structure; c – e) in sections of different thickness *t*: c) 0.1 µm, d) 1 µm, e) 4 µm; (rubber selectively stained, HVEM)

(the pole cap) is cut away. Only thicker sections show the true shape and size of the larger salami particles without deterioration. HVEM micrographs c–e in Fig. 9.3 reveal that with increasing section thickness t the particles appear better in their true shape and size. The true particle diameter of 1 μm (on average) is visible only in the thickest section (t = 4 μm). Using ultrathin sections with t = 0.1 μm, an average value of only 0.5 μm can be measured. When determining exact particle sizes and frequency distributions, it is notable that larger particles are visible in the ultrathin sections (approx. 100 nm thick) only as cross-sections, which are usually smaller than the real diameter (this effect is known as the "tomato salad problem"). A detailed analysis of rubber particle diameter distributions on 0.1 up to 4 μm thick sections in a 1000 kV–HVEM (as in Fig. 9.3) revealed deviations of more than 100 %. If the particles are larger than the section thickness, the measured frequency distribution is shifted to apparently smaller diameters [9, 10].

"Tomato salad problem"

Some types of rubber particles exhibit their own morphology, for instance CPE particles in ACS, acrylic rubber in PVC (see Fig. 9.33), or EP rubber in PP (see Fig. 9.4 b). In a blend with a semicrystalline matrix, the lamellar arrangement at the interface between matrix and particles depends on the degree of compatibility between the both phases. Figure 9.4 shows rubber toughened PP with EPDM and EPR particles. Lamellae of PP penetrate into the particle, indicating a good compatibility and phase connection. Inside the particles, some lamellae are visible due to the low but non-negligible crystallinity.

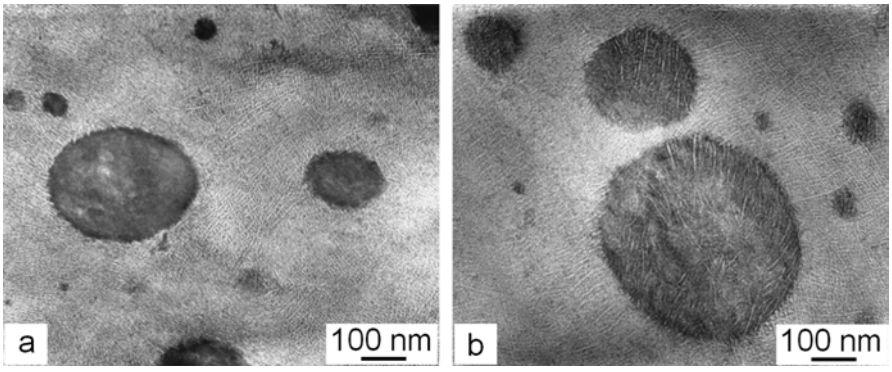

FIGURE 9.4 Rubber-toughened iPP with EPDM a) and EPR particles b) (stained ultrathin sections, TEM)

A rather different type of morphology is present in the network arrangement of the rubber in toughened PVC; here, very tiny rubber layers wrap around the primary PVC particles – see Fig. 1.29 (compare with the morphology of PVC in Fig. 6.14). An advantage of these systems (together with very high toughness – see below) is that only a small rubber content of less than 10 % is necessary to create the network. However, they also come with a strong disadvantage, because the network morphology is highly sensitive to processing [11, 12]. Therefore, these PVC network systems have no practical application today. However, it is shown in Section 9.5 that network morphologies possess some principal advantages and that they may possibly be realized again in connection with PS/PB block copolymers (see Section 11.2.5.3).

The transition in deformation behavior appearing in fibers thinner than 225 nm is sketched in Fig. 11.68.

To conclude, the usually brittle PS can be modified using electrospinning technique so that a transition from crazing behavior to micro-necking and ductile behavior occurs. The increased ductility of very thin PS fibers could be used to produce ductile PS networks for different applications, for instance networks as flocculants in the treatment of waste water [200], ion exchanger [201], for organic electronic applications [202], for optical application [203], and as scaffolds for biomedical applications [204].

11.4.5 Nanofibers – Nanocomposites

An additional advantage of electrospinning is the possibility to distribute nanoparticles without agglomeration (the main problem in the usual procedures to prepare nanocomposites it is to avoid agglomeration of nanoparticles – see Section 10.3). In Fig. 11.69, the morphology of a PMMA nanofiber filled with SiO_2 nanoparticles is shown as well as deformation after tension in fiber direction. The nanofiber-nanocomposite is deformed by necking and cold drawing. Similar effects have been found in polycarbonate/multiwalled carbon nanotubes [205] and in PMMA/montmorillonite nanocomposite nanofibers [206, 207].

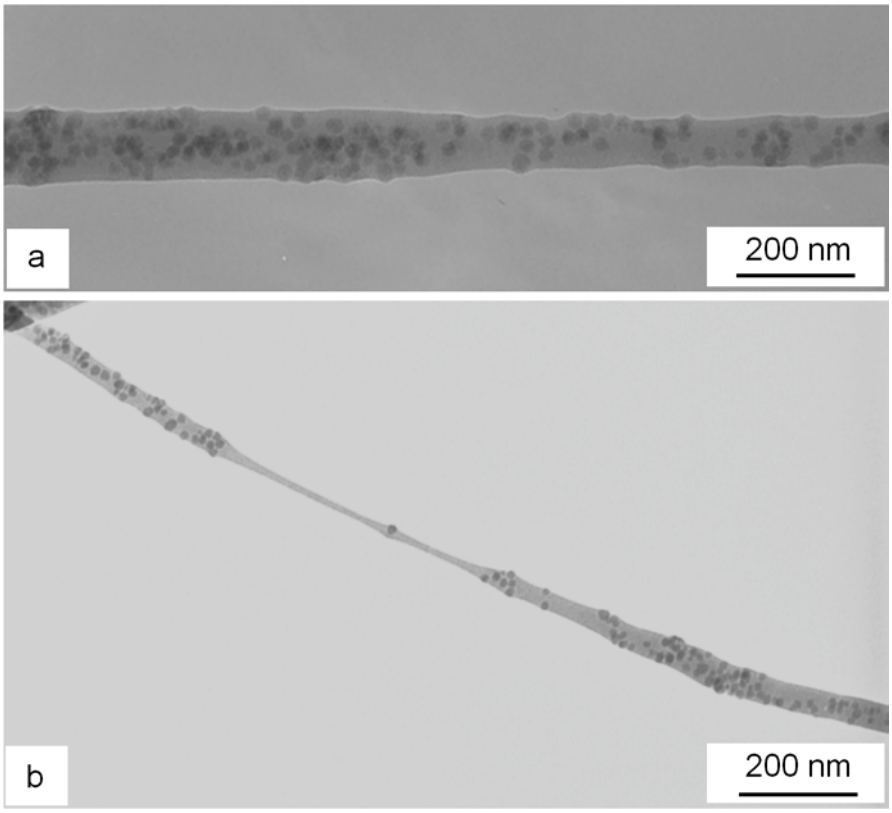

FIGURE 11.69 TEM micrographs of PMMA/SiO_2 (20 wt.%) nanofiber-nanocomposite; a) morphology; b) tensile deformation with necking and cold drawing (after [207])

These examples of unique change in deformation behavior offer the possibility that an intrinsic brittle material can be manipulated to be ductile without sacrificing its other properties through a well-controlled electrospinning process.

■ 11.5 Conclusions

Mechanical loading of materials and specimens with reduced size is often connected with two general changes in mechanical properties with decreasing sample size:

1. Due to the structural confinement, smaller specimens also contain smaller defects. Decreasing the size of the defects enhances the strength of a material. This general well-known effect is based on Griffith's theory (see Section 5.2, valid for all materials) and is sketched in Fig. 11.70. Depending on material type, processing or sample history, specimens contain typical minimum defects that limit strength (maximum stress σ_{max}). A material without any defects would reach the theoretical strength σ_{theor}.

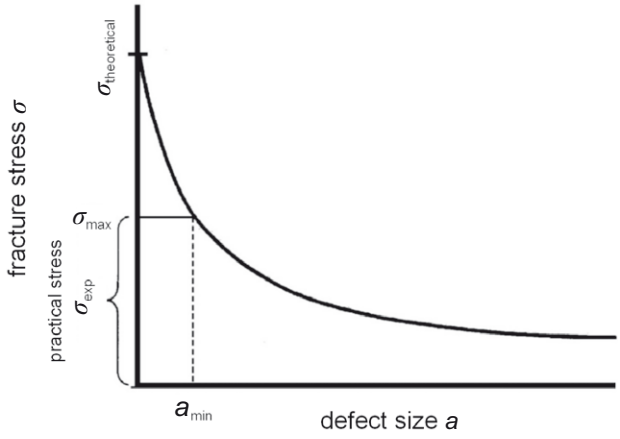

FIGURE 11.70 Influence of defect size in a material on strength. The practically usable region (region of practical, experimental stress σ_{exp}) up to a maximum stress σ_{max} is defined by typical smallest defects a_{min}; the theoretical maximum of the fracture stress σ_{theor} is calculated under the assumption of missing all defects in the material

2. The reduction of characteristic sizes of a material up to the nm-level may lead to the occurrence of new nanomechanical effects.

The second point due to nanomechanical effects is of particular interest, because it is not only the result of lack or reduction of defects, but also induces the appearance of a new quality of the material with a transition to new nano-effects with clear improvement in properties. Several nano-effects are known and have been discussed in the forgoing sections:

- In case of nanocomposites, the nanoparticles can modify the matrix polymer in a thin layer at the particle/matrix interface. Also, if such an interphase is very thin (range of 1 nm up to 10 nm), the total volume of all interphases can change the nanocomposite from a *matrix material* to an *interphase material* with corresponding changes in properties – see Section 10.3 with Figs. 10.16 and 10.17.

- In block copolymers with thin polystyrene and polybutadiene layers, a transition from the brittle craze-like deformation of PS to a ductile yielding occurs, if the PS layers are thinner than a critical thickness (approx. 25 nm at room temperature). This effect was called *thin layer yielding* and is discussed in Section 11.2 and illustrated in Figs. 11.12 and 11.15.
- Coextruded multilayered polymer systems with PS or PMMA layers reveal a transition from brittle behavior of the glassy polymer to a ductile deformation by necking and cold drawing. Examples are discussed in Section 11.3 and illustrated in Figs. 11.48 and 11.49.
- Electrospun nanofibers of PS reveal a brittle-ductile transition (with transition from craze-like deformation to necking and cold drawing) if the PS nanofibers are thinner than 225 nm at room temperature. Such an effect was also detected in nanofiber nanocomposites, e. g., PMMA nanofibers with SiO_2 nanoparticles – see Sections 11.4.4, 11.4.5, and Figs. 11.66, 11.68, and 11.69.

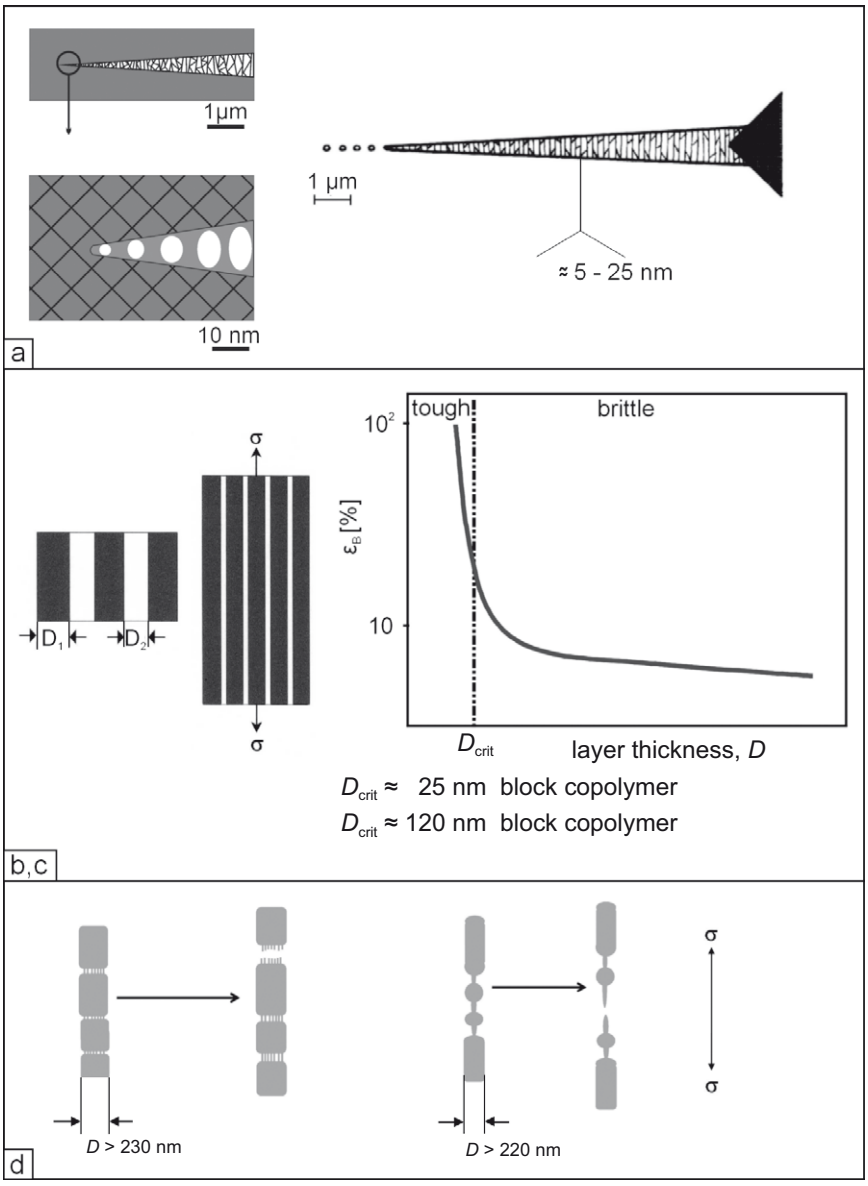

FIGURE 11.71 Schematics of different size-dependent brittle-tough transitions in nanostructured polymers; a) crazing in amorphous brittle polymers; b), c) thin layer yielding in block copolymers and coextruded multilayered polymers; d) cold-drawing in nanofibers

The common result of all of these effects is that transitions leading to an improved ductility (elongation at break, toughness) occur, if polymer layers or fibers are thinner than a critical size *(size-dependent brittle–tough transition)*. The ability of brittle polymers to exhibit intrinsic ductility has been known for many years from the effect of stretching fibrils inside the crazes (in PS-crazes the craze fibrils are stretched up to about 300% – this is the limit of stretching the entanglement network, see Section 4.4. and Figs. 4.19–4.22). The different mechanisms of a *size-dependent brittle–tough transition* are sketched in Fig. 11.71. Figure 11.71 (a) illustrates the formation of the about 5–25 nm thick craze-fibrils with the stretching of the entanglement network (yielding up to the maximum of about 300%). Figure 11.71 (b, c) illustrates multilayered systems as in block copolymers (where PS layers covalently bonded to PB layers) and in coextruded systems (where PS layers are attached to PP layers, adhesion by van der Waals forces). In Fig. 11.71 (d) the situation of PS nanofibers is sketched with appearance of usual crazing in thicker fibers (thickness >230 nm) and transition to necking and cold-drawing in thin fibers (thickness <220 nm). Table 11.1 summarizes these different nanomechanical effects with the critical sizes or layer thicknesses and correlates them with the type of interface at the yielding polymer part (a – d correlate with a – d in Fig. 11.71).

TABLE 11.1: Summary of Nanomechanical Effects, Type of Interface with Acting Forces and Critical Sizes of the Thin PS Parts (Fibers, Layers) at Room Temperature

Nano-effect	Interface/nature of forces	Critical size
a) Stretching of fibrils in PS crazes	PS material/entanglements of PS	20–25 nm
b) Thin layer yielding in SB blockcopolymers	Polybutadiene-rubber layers/covalent bonds	25 nm
c) Yielding of PS multilayers in coextruded materials	Ductile (PP) layers/van der Waals forces	120 nm
d) Yielding of PS nano-fibers	Air/-	225 nm

In highly entangled and covalently bonded materials only very small layers or fibrils can yield. Stretching of craze fibrils occurs only after local nanovoiding in the pre-crazes with characteristic distances of 20–30 nm and, correspondingly, polymer strands between them in the same order of magnitude. It is to be assumed that the conformation of the PS macromolecules in the layers of the SB block copolymers is similar to that in bulk PS. Therefore, the transition to yielding should occur in the same thickness range as for the fibrils in crazes, i.e., at critical thicknesses of approx. 25 nm. In coextruded multilayer systems, the PS layers are not chemically bonded and attached to the neighboring layers only by weak van der Waals forces at the surfaces. It is known that surface layers contain loosely packed molecules with an increased free volume content, a decreased glass transition temperature [208] and, therefore, that they possess a lower yield stress. Freely grown nanofibers are not hindered in mobility at the surface and, consequently, should exhibit an additional reduction of yield stress.

Estimation of the critical thickness

If we assume that the critical thickness of a plastically deformable PS layer is 25 nm (as in craze fibrils and block copolymer layers), then it can be concluded that in coextruded multilayers the modified surface layers with a lower yield stress are in the thickness range of approx. 50 nm (50 ≈ ½ (120 – 25)). The determined larger critical size of PS nanofibers (225 nm instead of 120 nm) could be correlated to the absence of the constraint effect of neighboring layers. In layers, an applied stress induces lateral constraint stresses perpendicular to the applied load, which reduces the original stress; therefore, a larger applied stress is necessary to reach the yield stress of the material. On the other hand, the nanofibers should possess a molecular orientation in the fiber axis, which would result in an increased yield stress.

The critical thickness of approx. 25 nm for yielding (craze fibrils and thin layers) was correlated with the entanglement model (Figs. 1.10 and 4.19) [142]. Let us consider a thin polymer sample with the thickness of only the diameter of the macromolecular coils in commercial PS, i. e., the mesh size of the entanglement network – as it is sketched in Fig. 11.72 at the top left. In this situation, stress transmission through entanglements only occurs in the direction of stress, creating a state of plane stress. It is clear that in such an arrangement lateral constraints are totally absent and macromolecules can be oriented and plastically stretched to the maximum extension ratio $\lambda_e \approx 4$ (see Section 4.4) without formation of voids, crazes, or cracks. If we increase the layer thickness and reach twice the mesh size, some entanglements will point to the lateral direction. Due to these lateral constraints, the applied stress is reduced. In fully elastic media, an applied stress σ_0 initiates lateral (or transverse) stresses $\sigma_t = \nu \cdot \sigma_0$ (ν = Poisson's constant), which are acting back on the applied stress, reducing it by a factor of $\nu \cdot \sigma_t = 2\,\nu^2\,\sigma_0$. With the usual value of Poisson's constant of $\nu = 0.3$, the effective applied stress σ_t will be reduced to $0.8\,\sigma_0$. To reach the level of the original yield stress σ_y, a larger applied stress would be necessary. In addition, the uniaxial stress state (such as in craze fibrils and thin strands) is transformed into a triaxial stress state. The change of local stresses with increasing layer thickness D is schematically shown in Fig. 11.72. The transverse stress obviously increases most notably in the range of D between one and two mesh diameters, i. e., between 15 and 30 nm in PS.

Thin layer yielding as a basic effect of brittle-tough transitions

Consequently, the apparently different nanomechanical mechanisms of *size-dependent brittle–tough transitions* are based on the same nanomechanical effect of ductility, the *thin layer yielding*. The critical size or thickness of the transition from brittle into ductile behavior depends on the specific polymer, the temperature, and the surrounding, i. e., the attached material. The occurrence of this effect in several different polymers gives rise to hope that it can be also applied in other polymer systems to improve ductility and toughness in combination with good stiffness and strength. Therefore, using the knowledge on nanostructure and nanomechanical effects can help to exploit the full potential of polymers for new and broader applications.

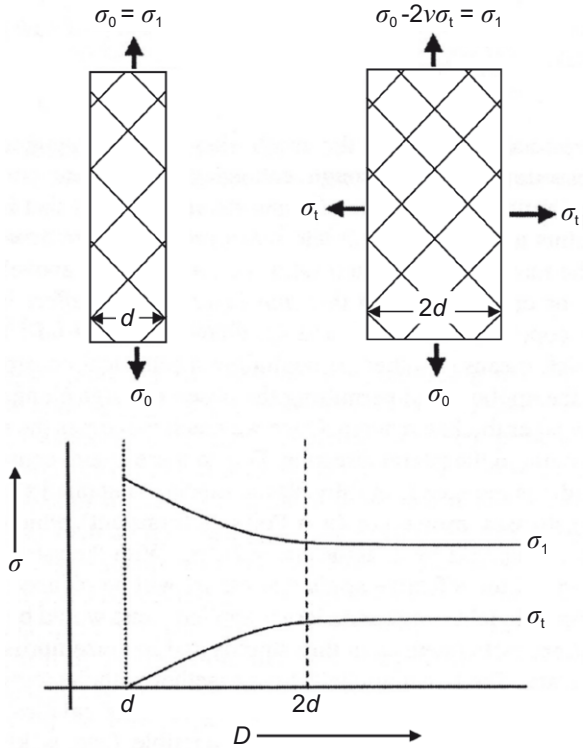

FIGURE 11.72 Changes of stresses in an entangled network with increasing layer thickness; σ_0 = applied load, σ_1 = stress component in direction of load, σ_t = stress component in transverse direction (after [142])

References

1. Hamley, I. W.: The Physics of Block Copolymers, Oxford Publishers, Oxford, 1998.
2. Bates, F. S.; Fredrickson, G. H.: *Ann. Rev. Phys. Chem.* **41** (1990) p. 525–57.
3. Hasegawa, H.; Hashimoto, T.: Self assembly and morphology of block copolymer systems, in Aggarwal, S. L.; Russo, S. (Eds.), Comprehensive Polymer Science, Supplement 2, Pergamon, London, 1996.
4. Adhikari, R.; Michler, G. H.: *Prog. Polym. Sci.* **29** (2004) p. 949–986.
5. Ruzette, A.-V.; Leibler, L.: *Nat. Mater.* **4** (2005) p. 19–31.
6. Milner, S. T.: *Macromolecules* **27** (1994) p. 2333–2335.
7. Quirk, R. P.; Morton, M.: in Holden, G.; Legge, N. R.; Quirk, R. P.; Schroeder, H. E. (Eds.): Thermoplastic Elastomers, 2nd Edition, Hanser Publishers, Munich 1998.
8. Drolet, F.; Fredrickson, G. H.: *Phys. Rev. Lett.*, **83** (1999) p. 4317–4320.
9. Matsen, M. W.: *J. Chem. Phys.* **113** (2000) 5 p. 539–5544.
10. Davis, K. A.; Matyjaszewski, K.: *Adv. Polym. Sci.* **159** (2002) p. 107–170.
11. Mori, Y.; Lim, L. S., Bates, F. S.: *Macromolecules* **36** (2003) p. 9879–9888.
12. Hamley, I. W. (Ed.): Developments in Block Copolymer Science and Technology, Wiley InterScience, New York 2004.
13. Holden, G.: Understanding Thermoplastic Elastomers, Hanser Verlag, Munich 2000, p. 15–35.
14. Baltá-Calleja, F. J.; Fakirov, S.: The Microhardness of Polymers, Cambridge University Press, Cambridge 2000.
15. Flores, A.; Ania, F.; Baltá-Calleja, F. J.: *Polymer* **50** (2009) p. 729–746.
16. Michler, G. H.; Baltá-Calleja, F. J.; Adhikari, R.; Knoll, K.: *J. Mater. Sci.* **38** (2003) p. 4713–4723.